

Merrifield Resin-based Imine Compounds and their Co(II), Ni(II) and Cu(II) Complexes: Characterization and Study of their Catalytic Activities

Elif Sari^{1,a} · Mustafa Bal^{2,b,*} · Mehmet Tümer^{3,c}¹ Chemistry Department, Kahramanmaraş Sutcu Imam University, Kahramanmaraş, Türkiye.² Department of Machinery and Metal Technologies, Airbus-TUSAŞ Aviation Vocational School, Kahramanmaraş İstiklal University, Kahramanmaraş, Türkiye.³ Chemistry Department, Kahramanmaraş Sutcu Imam University, Kahramanmaraş, Türkiye.

*Corresponding author e-mail address: mustafabal46@gmail.com

Research Article

History

Received: 08.10.2025


Accepted: 23.03.2026



This article is licensed under a Creative Commons Attribution-NonCommercial 4.0 International License (CC BY-NC 4.0)

ABSTRACT

In the current study, three new polymer- attached imine ligands (PS-L¹—PS-L³) were synthesized from the reaction of chloromethyl polystyrene and the imine compounds (H₂L¹—H₂L³). The Co²⁺, Ni²⁺ and Cu²⁺ complexes of the polymer- attached ligands were prepared and characterised by the spectroscopic procedures. The redox and photophysical behaviours of the free imine ligands were investigated in solutions. Polymer supported ligands (PS-L¹—PS-L³) and their Co²⁺, Ni²⁺ and Cu²⁺ complexes show good high thermal stabilities. Alkane-oxidation and alkene-epoxidation studies of solid supported metal complexes were carried out by microwave method. In the oxidation studies of the cyclohexane (CYH) and cyclooctane (C₈H₁₆) (CYON), the complexes showed good catalytic conversion rate (up to 90%) but with lower selectivity.

Keywords: Catalytic conversion, Epoxidation, Heterogenous catalyst, Oxidation, Polymer- attached imines^a  0009-0008-8507-5058^c  0000-0002-1882-429X^b  0000-0003-2576-3947

1. Introduction

Please Imine compounds play a key role in the preparation of industrially important chemicals by using them as substrates in many different reactions [1]. Since these compounds contain heteroatoms such as nitrogen and oxygen, they form metal complex compounds with transition metal ions [2]. Due to the fact that these compounds have these properties, they have made very important contributions to the development of coordination chemistry [3]. However, concrete and rapid advances in this field did not become apparent until the 1950s [4,5]. After the introduction of imine compounds in the literature, at first all efforts were focused only on the synthesis and characterization of their metal complexes [6]. In later periods, the application areas of imine compounds and transition metal complexes were investigated, and it was determined that these materials have main biological activities [7] such as antimicrobial, antifungal, antitumor, and herbicide [8]. In addition, it has been determined that imine compounds can be used as analytical purification tools due to their metal binding properties [9,10].

Obtaining and characterizing metal complexes of polymeric ligands is extremely important in terms of chemistry [11,12]. In a polymeric material, the structural environment of the material function is one of the basis factors directing the complexation with metal ions [13,14]. The characteristics of functional polymers are not only derived from the macromolecular structure but

depends to a significant extent on the functional group substitution in the macromolecules [15,16]. The chemistry, synthesis, structural modification and applications of functional polymers in chemistry have recently become the focus of attention [17]. The binding of low molecular weight ligands to the macromolecular matrix insoluble in organic or inorganic solvents can also solve the problems of instability, toxicity or odour often experienced with low molecular weight reagents [18,19]. On the other hand, the polymeric matrix can be chosen or custom made to provide a specific microenvironment that can induce some specificity in the reaction site [20]. Because of the possibility of incorporating a number of functional groups by the nucleophilic displacement of chlorine, polystyrene is the most commonly used support in reactive polymers [21]. Polymer supported chelating agents form an important group of compounds for the complexation of metal ions in the separation chemistry [22].

In this article, polymer- attached imine ligands (PS-L¹—PS-L³) were obtained from the synthesized H₂L¹—H₂L³ compounds, and Co²⁺, Cu²⁺, and Ni²⁺ complexes were synthesized. Structural characterization of the synthesized products was performed using spectroscopic and analytical instruments. Oxidation and epoxidation studies were conducted using polymeric transition metal complexes as catalysts.

2. Materials and Methods

2.1. Synthesis of H₂L¹-H₂L³

Schiff base ligands were synthesized according to the literature. 350 mg 2,4-Dihydroxybenzaldehyde (2 mmol) dissolved in 20 mL anhydrous ethanol and 74 mg 1,3-diaminopropane (H₂L¹) (1 mmol), 74 mg 1,2-diaminopropane (H₂L²) (1 mmol) and 103 mg diethylenetriamine (H₂L³) (1 mmol) dissolved in 20 mL ethanol were combined in a flask and refluxed at 85 °C for approximately 4 hours [23]. Color (C), Yield (Y), Melting point (MP), M.W, Elemental analysis (EA) (Found and Calculated) values are given respectively.

H₂L¹: C: Yellow, Y: 97%, MP: 186 °C, M.W: 314 g/mol. EA: % Found (% Calculated): C, 59.13 (64.96); H 5.903 (5.77); N 8.422 (8.91). FTIR (KBr, cm⁻¹): 3100 ν(OH), 1634 ν(CH=N), 1235 ν(C-OH). UV-vis (λ_{max}, nm, DMF, 1x10⁻³ M): 317, 387. ¹H-NMR (δ, ppm, DMSO-d₆): 3.44-3.58 (6H, m, CH₂), 6.18-7.18 (6H, m, Ar-H), 8.4 (2H, s, CH=N), 13.95 (4H, br, OH). ¹³C-NMR (δ, ppm, DMSO-d₆): 32.18-54.84 (CH₂), 103.10-162.39 (Ar-C), 165.51 (CH=N). LC-MS (e/m): 314 [M]⁺ (5%), 315 [M+1]⁺ (100%), 316 [M+2]⁺ (30%), 221[C₁₁H₁₃N₂O₃]⁺ (20%).

H₂L²: C: Dark yellow, Y: 77%, MP: 290 °C, M.W: 314 g/mol. EA: Found% (Calculated): C, 65.86 (64.96); H 6.064 (5.77); N 8.49 (8.91). FTIR (KBr, cm⁻¹): 3115 ν(OH), 1639 ν(CH=N), 1225 ν(C-OH). UV-vis (λ_{max}, nm, DMF, 1x10⁻³ M): 240, 312, 388. ¹H-NMR (δ, ppm, DMSO-d₆): 3.42-3.72 (6H, m, CH₂), 6.15-7.15 (6H, m, Ar-H), 8.32-8.36 (2H, s, CH=N), 13.69 (4H, br, OH). ¹³C-NMR (δ, ppm, DMSO-d₆): 20.43-63.85 (CH₂), 102.93-162.31 (Ar-C), 165.13-166.25 (CH=N). LC-MS (e/m): 315 [M+1]⁺ (55%), 316 [M+2]⁺ (100%), 317 [M+3]⁺ (20%), 221[C₁₁H₁₃N₂O₃]⁺ (25%).

H₂L³: C: Dark yellow, Y: 96%, MP: 280 °C, M.W.: 343 g/mol. EA: Found% (Calculated): C, 61.35 (62.96); H 6.520 (6.16); N 10.65 (12.24). FTIR (KBr, cm⁻¹): 3180 ν(OH), 3112 ν(N-H), 1634 ν(CH=N), 1221 ν(C-OH). UV-vis (λ_{max}, nm, DMF, 1x10⁻³ M): 261, 303, 383. ¹H-NMR (δ, ppm, DMSO-d₆): 3.44-3.55 (8H, m, CH₂), 6.11-7.11 (6H, m, Ar-H), 8.26 (2H, s, CH=N), 13.68-13.87 (4H, br, OH). ¹³C-NMR (δ, ppm, DMSO-d₆): 49.93-56.69 (CH₂), 103.31-162.65 (Ar-C), 166.90 (CH=N). LC-MS (e/m): 343 [M]⁺ (20%), 345 [M+2]⁺ (10%), 325 [C₁₈H₁₉N₃O₃]⁺ (13%).

2.2. Synthesis of Polymer- Attached Schiff Bases (PS-L¹–PS-L³)

Merrifield peptide resin (PS) (2% cross-linked with 3.9 mmol Cl and divinylbenzene per g resin) (2.0 g) was swollen in DMF (40 ml) for 1 h, and solutions of H₂L¹-H₂L³ (3.14 g, 10.0 mmol, 3.43 g, 10.0 mmol, respectively) in methanol (25 ml) and DMF (15 ml) were added. After adding 50 mL of ethanol and 2 mL of triethylamine to the mixture, the system was refluxed for 48 h. As a result of this prolonged heating period, the visual state of the polymer changed; its bright yellow color turned dark brown.

PS-H₂L¹: C: Brown, Y: 87%, m.p.:> 250 °C. EA: Found%: C, 70.76; H, 6.29; N, 1.32. FTIR (KBr, cm⁻¹): 3162 ν(OH), 1594 ν(CH=N), 1224 ν(C-OH).

PS-H₂L²: C: Brown, Y: 60%, m.p.:> 250 °C. EA: Found%: C, 84.11; H, 7.03, N, 1.42. FTIR (KBr, cm⁻¹): 3110 ν(OH), 1601 ν(CH=N), 1264 ν(C-OH).

PS-H₂L³: C: Dark brown, Y: 8%3, m.p.:> 250 °C. EA: Found%: C, 73.16; H, 6.49; N, 1.64. FTIR (KBr, cm⁻¹): 3228 ν(OH), 3050 ν(N-H), 1586 ν(CH=N), 1222 ν(C-OH).

2.3. Co²⁺, Cu²⁺ and Ni²⁺ Complexes of Polymer-attached Schiff Bases

Polymer- attached Schiff bases were converted to metal complexes by suspension in methanol and mixing with hot solutions of Copper (II), Cobalt (II), and Nickel (II) salts. The reaction was carried out over a time period of 8 h and a controlled nitrogen environment with reflux heating was used during this process.

2.4. Alkane-Oxidation and Alkene-Epoxidation in Microwave Radiation Environment

Microwave-assisted catalytic oxidation and epoxidation experiments were carried out using cyclohexane(C₆H₁₂), cyclooctane(C₈H₁₆), cyclohexene (C₆H₁₀), and styrene substrates. For each experiment, 0.02 mmol of the catalyst complex was dissolved in acetonitrile (5 mL), and then 2 mmol of substrate and 4 mmol of H₂O₂ were added to prepare microwave vessels. The vessels were immediately sealed, placed in a Berghof MWS3+ microwave oven, and irradiated at 400 W (40% of maximum power) for 60 min. Although the microwave system automatically controlled the temperature at approximately 140 °C, the temperature briefly reached 150–160 °C due to evaporation of the solvent and substrate, and the pressure increased to 30–35 bar, respectively. First, an extraction with 10 mL of CH₂Cl₂ was performed to remove products other than organic acids. This was done after the reaction was stopped by adding 1 mL of water. The extract was then submitted to gas chromatography (GC) and GC-MS for detailed analysis. The amounts of products formed in the experiments, including CyH, Cy-OH, Cy=O, CyON, CyON-OH, CyON=O, C₆H₁₂ epoxide, and styrene epoxide were calculated using previously prepared external calibration curves. This method enabled the use of H₂O₂ as a green oxidant, a key advantage of the catalytic system. The study aimed to develop an efficient and environmentally friendly process to produce valuable chemicals.

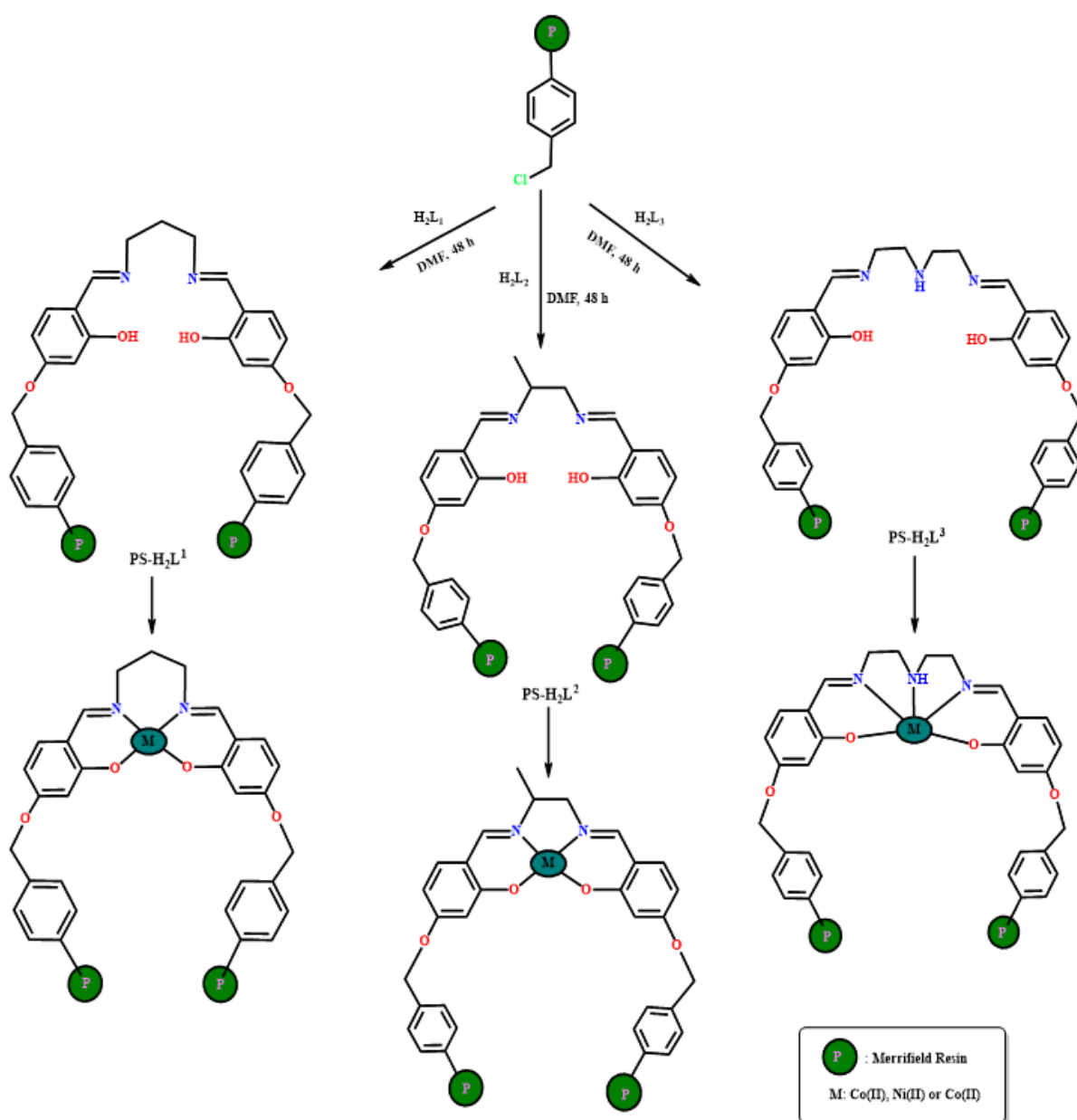
Comparing the catalytic performance of the synthesized polymer-supported Cu(II) and Co(II) complexes with previously reported heterogeneous systems, it is observed that our catalysts exhibit highly competitive conversion rates. For instance, the ~90% conversion rate achieved in the oxidation of cyclohexane under microwave-assisted conditions compares favorably with the 75–85% conversion ranges typically reported for conventional zeolite or polymer-supported transition metal catalysts [24,25]. This enhanced activity can be attributed to the well-defined coordination environment

of the Schiff base ligands on the Merrifield resin, which facilitates efficient substrate access to the metal centers [26,27].

3. Results and Discussion

In this research, firstly, we synthesized three polydentate compounds $H_2L^1-H_2L^3$ from the reactions of the primary diamines and 2,4-dihydroxy benzaldehyde in the ethanol. Ligands were characterized by the spectroscopic and analytical technique. Analytical and spectroscopic data of compounds are given in the experimental section.

Merrifield resin polymer is a cross-linked polymer with chloromethyl functional groups. It can be used as a solid support material by reacting over the chloromethyl functional group. For this purpose, the organic compounds containing -OH or -NH₂ substitute groups are reacted with Merrifield resin polymer and polymer supported materials are obtained. In this study, imine compounds ($H_2L^1-H_2L^3$) containing hydroxyl groups to react with the polymer were synthesized and analyzed in detail using different spectroscopy methods. Since Merrifield resin polymer is cross-linked, it has little solubility and swelling even in the DMF solvent medium. Polymer supported imine compounds ($PS-L^1-PS-L^3$) were obtained from the reaction between imine compounds and Merrifield resin in DMF solvent medium (Figure 1).



3.1. FTIR Spectrum Analysis of Materials

In infrared spectra of the materials, the $\nu(\text{OH})$ vibrations were observed in 3400-3200 cm^{-1} range. In the spectrum of the H_2L^3 ligand, band at 3180 cm^{-1} belongs to the secondary amine (-NH) group. The strong bands in the 1639-1634 cm^{-1} range may be assigned to the vibrations of the azomethine groups. The phenolic (C-OH) vibrations were seen in the range of 1362-1355 cm^{-1} .

In the FTIR spectra of the polymeric ligands ($\text{PS-L}^1\text{—PS-L}^3$), the vibrations in the range of 3228-3110 cm^{-1} belong to the $\nu(\text{OH})$ group. In the PS-L^3 spectrum, the band at 3050 cm^{-1} belongs to the $\nu(\text{NH})$ stretching. The bands in the range of 1601-1586 cm^{-1} belong to the $\nu(\text{CH=N})$ group.

The Ni^{2+} , Cu^{2+} and Co^{2+} complexes of the polymer-attached Schiff bases were synthesized and characterized. The obtained spectral data of complexes are shown in Table 1. In the spectra of the complexes, the bands in 3384-3286 cm^{-1} can be attributed to the $\nu(\text{H}_2\text{O})$ vibration. The $\nu(\text{CH=N})$ vibrations were shown in the 1582-1601 cm^{-1} range. The phenolic $\nu(\text{C-OH})$ stretching are shown in 1264-1224 cm^{-1} range. In the complexes, two new bands occurred in the far region. These bands are in the 580-572 cm^{-1} range $\nu(\text{M-O})$ and 435-430 cm^{-1} range $\nu(\text{M-N})$ vibrations, respectively.

Table 1. The FTIR spectral data of the polymer-attached Schiff base complexes (cm^{-1}).

Compound	Color	$\nu(\text{H}_2\text{O})$	$\nu(\text{CH=N})$	$\nu(\text{C-OH})$	$\nu(\text{M-O})$	$\nu(\text{M-N})$	$\mu_{\text{eff}}(\text{B.M.})$
$\text{PS-L}^1\text{-Co (II)}$	Brown	3384	1600	1225	580	435	0.24
$\text{PS-L}^1\text{-Cu (II)}$	Brown	3324	1600	1228	575	430	0.23
$\text{PS-L}^1\text{-Ni (II)}$	Brown	3286	1600	1224	577	432	-
$\text{PS-L}^2\text{-Co (II)}$	Brown	3316	1599	1228	565	425	0.21
$\text{PS-L}^2\text{-Cu (II)}$	Brown	3324	1600	1228	570	428	0.24
$\text{PS-L}^2\text{-Ni (II)}$	Brown	3321	1600	1223	572	430	-
$\text{PS-L}^3\text{-Co (II)}$	Brown	3388	1601	1264	576	435	1.27
$\text{PS-L}^3\text{-Cu (II)}$	Brown	3349	1582	1260	575	430	0.50
$\text{PS-L}^3\text{-Ni (II)}$	Brown	3301	1601	1264	580	430	-

In the spectra of solid-supported ligands, some broad absorption bands originating from the hydroxyl (OH) group disappeared and the characteristic vibration bands of the azomethine (CH=N) group were observed to shift to the lower 10-20 cm^{-1} regions. In the spectra of the complexes, in addition to the characteristic vibration bands of the ligands, metal-oxygen and metal-nitrogen vibration bands were observed in the range of 540-420 cm^{-1} . To better characterize the M-N and M-O vibration bands, FT-flash spectra of solid-supported transition metal complexes were examined. The M-O band was observed in the range of 340-300 cm^{-1} , and the M-N vibration bands were observed in the range of 280-90 cm^{-1} .

3.2. UV-vis Spectra Analysis of Materials

Within the scope of the study, electronic absorption spectral data of solid-supported ligands and metal complex compounds synthesized were examined in DMF solution. In the spectra of the ligands, the absorption bands at 240 and 261 nm can be attributed to $\pi\text{-}\pi^*$ transitions. The bands observed in the range of 388-303 nm were assigned to $n\text{-}\pi^*$ transitions. The absorption

wavelengths of the compounds are shown in Table 2. UV-vis spectra of solid-supported ($\text{PS-H}_2\text{L}^1$), ($\text{PS-L}^1\text{-Co}$), ($\text{PS-L}^1\text{-Cu}$) and ($\text{PS-L}^1\text{-Ni}$) compounds are shown in Figure 2.

Table 2. UV-vis spectra data of compounds (nm).

Compounds	λ_{max} (nm)
$\text{PS-H}_2\text{L}^1$	317, 387
$\text{PS-L}^1\text{-Co}$	290, 312, 387, 603, 679
$\text{PS-L}^1\text{-Cu}$	219, 321, 452, 599
$\text{PS-L}^1\text{-Ni}$	242, 310, 392, 608
$\text{PS-H}_2\text{L}^2$	240, 312, 388
$\text{PS-L}^2\text{-Co}$	605, 673
$\text{PS-L}^2\text{-Cu}$	260, 309, 361, 367, 386, 513
$\text{PS-L}^2\text{-Ni}$	376, 391, 435, 550
$\text{PS-H}_2\text{L}^3$	261, 303, 383
$\text{PS-L}^3\text{-Co}$	246, 300, 389, 511, 599, 673
$\text{PS-L}^3\text{-Cu}$	251, 284, 306, 370, 448, 570
$\text{PS-L}^3\text{-Ni}$	245, 291, 384, 614

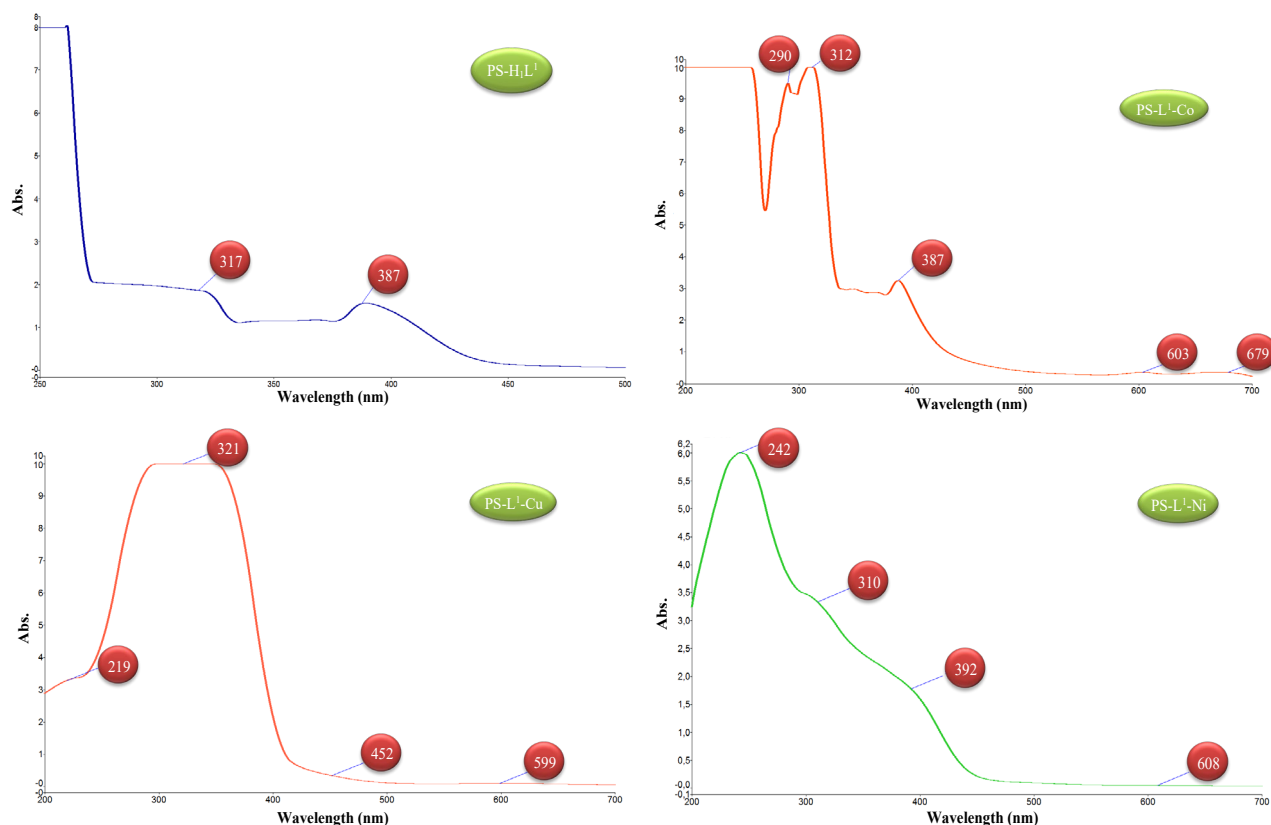


Figure 2. UV-vis spectra of (PS-H₂L¹), (PS-L¹-Co), (PS-L¹-Cu) and (PS-L¹-Ni) compounds.

3.3. NMR Spectra of Materials.

In order to clarify the structures of compounds, ¹H and ¹³C NMR spectra were examined in DMSO-d₆ solvent environment. In the ¹H spectra of the ligands, the phenolic OH protons were seen in 13.68-13.97 ppm range as broad signal. The singlets of the protons of the azomethine groups were seen in 8.32-8.45 ppm range. Multiplets in 6.11-7.75 ppm range can be attributed to the aromatic ring protons. The multiplets in 1.06-3.72 ppm are assigned to the protons of methylene groups.

In ¹³C NMR spectra of materials, the observed signals in the 165.13-166.90 ppm can be attributed to the carbons of the azomethine groups. Aromatic ring carbon atoms were seen in the 102.94-162.14 ppm range. Signals in the range of 20.43-63.85 ppm belong to aliphatic carbon atoms.

3.4. Mass Spectra of Materials

The chemical formulation of the ligands was determined primarily based on elemental analysis and ¹H(¹³C) NMR data. In addition to these findings, mass spectroscopy results were also included in the experimental part to support the formulation. The mass spectra of H₂L¹ and H₂L³ show [M+1]⁺, peaks at m/e 314 (%5) and 343 (%13), respectively, while the ligand H₂L² has not molecular ion peak. The ligands H₂L¹-H₂L³ show fragmentation peaks [M+1]⁺ at m/e = 315 (%100), 315 (%55) and 345 (%10), respectively. In mass spectra of ligands H₂L¹ and H₂L², the peak at m/e = 221 can be attributed to the [C₁₁H₁₃N₂O₃]⁺ ion occurring by loss of the [C₆H₅O]⁺ ion from the ligands. In spectrum of H₂L³, peak at m/e 325 due to the [C₁₈H₁₉N₃O₃]⁺ ion. The spectra of all the images examined show striking similarity, suggesting their structural proximity to persistent complexes. The fragmentation rates observed in mass spectroscopy are similar for all complexes, suggesting some common steps.

3.5. Photoluminescence Spectral Studies

The photoluminescence properties of ligands H₂L¹-H₂L³ were studied in EtOH, CH₃CN, MeOH and DMF solvents using 1.0×10^{-3} - 1.0×10^{-7} M solutions. Emission and excitation spectra of H₂L¹ in MeOH are shown in Figure 3. The emission and excitation data of the materials are given in Table 3. The spectra of ligands show one emission band in the 680-602 nm range longer wavelength (LW) region in the DMF, MeOH, EtOH and CH₃CN solutions. Emission peaks of ligands in the ethanol solution were shifted to the shorter wavelengths. On the other hand, in MeOH and CH₃CN solutions, emission bands of compounds were shifted to the longer wavelengths. The photoluminescence emission peaks of ligands exhibit a significant redshift with the addition of electron-donating groups. Thanks to these additions, which occur through mesomeric and inductive effects, the δ - π hyperconjugation distribution allows the electrons from the phenyl exchange to be reduced, resulting in a redshift of the luminescence peaks in the 40-45 nm range. Methoxy-substituted ligands enhance photoluminescence emission through p- π conjugation, while p-hydroxy-substituted ones exhibit strong conjugation and a rigid planar structure. Furthermore, the adaptation spectra of plants H₂L¹-H₂L³ were investigated in solutions (DMF, CH₃CN, EtOH, and MeOH), and achieved data are presented in Table 3. The excitation spectra of the compounds resemble each other. In the excitation spectra of the ligands, the excitation peaks were shown in 567-545 nm range. Excitation peaks were shifted to the lower wavelengths of the ligand H₂L³. In the spectra of the L¹ material, the peaks consist of the strong π - π^* band with the long-wavelength edge at \sim 545 nm and a weak intra ligand charge transfer (ILTC) band with the edge at \sim 566 nm. Under increased polarity conditions, extended π -conjugation could cause the methoxy groups to contribute an excited-state resonance contribution to the benzene rings.

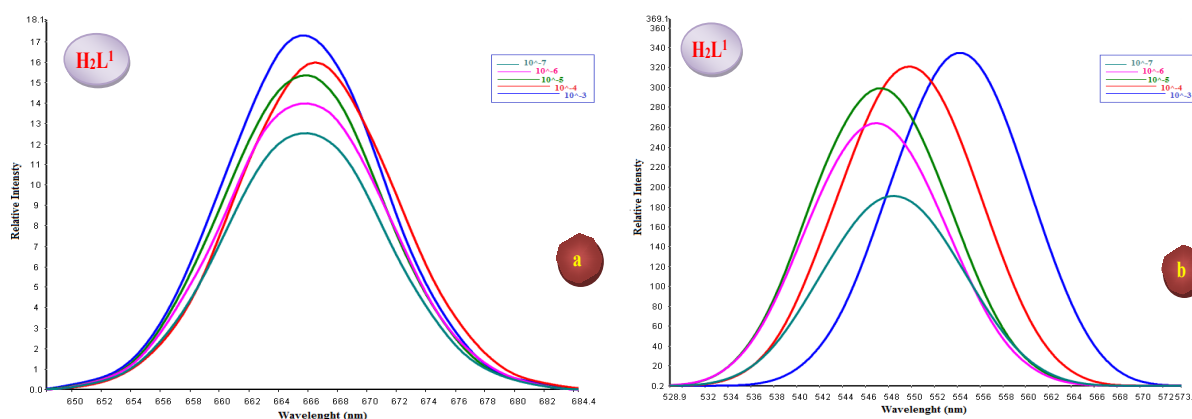


Figure 3. (a) Excitation spectrum and (b) emission spectrum of the H₂L¹ ligand in MeOH.

To understand the photoluminescence properties of some ligands H₂L¹-H₂L³ under influence of them, solutions in DMF, CH₃CN, EtOH and MeOH in solvents ranging from 1.0x10⁻³ M to 1.0x10⁻⁷ M were available. In the spectra of the compounds, it was observed that the emission peaks shifted to shorter wavelengths (towards blue) as the coverage decreased from 1.0x10⁻³ M to 1.0x10⁻⁷ M. A

significant decrease in the layers of absorption bands at lower wavelengths was also observed. This could be directly exploited with the structure of the substance content in the solution. Similarly, the same properties were exhibited at the adaptation points. Spectral data of the emission and excitation spectra of H₂L² and H₂L³ in various solvents are presented in Table 3.

Table 3. Excitation and emission spectral data of H₂L¹-H₂L³ Ligands in different solvent environments and at different concentrations.

Comp.	Conc.(M)	Solvent	Ex.(nm)	Em.(nm)	Comp.	Conc.(M)	Solvent	Ex.(nm)	Em.(nm)
H ₂ L ¹	1x10 ⁻³	CH ₃ CN	567	672	H ₂ L ²	1x10 ⁻³	EtOH	548	602
H ₂ L ¹	1x10 ⁻⁴	CH ₃ CN	552	662	H ₂ L ²	1x10 ⁻⁴	EtOH	550	604
H ₂ L ¹	1x10 ⁻⁵	CH ₃ CN	551	660	H ₂ L ²	1x10 ⁻⁵	EtOH	549	607
H ₂ L ¹	1x10 ⁻⁶	CH ₃ CN	547	659	H ₂ L ²	1x10 ⁻⁶	EtOH	547	612
H ₂ L ¹	1x10 ⁻⁷	CH ₃ CN	546	659	H ₂ L ²	1x10 ⁻⁷	EtOH	548	613
H ₂ L ¹	1x10 ⁻³	DMF	547	680	H ₂ L ²	1x10 ⁻³	MeOH	545	667
H ₂ L ¹	1x10 ⁻⁴	DMF	547	665	H ₂ L ²	1x10 ⁻⁴	MeOH	547	666
H ₂ L ¹	1x10 ⁻⁵	DMF	547	662	H ₂ L ²	1x10 ⁻⁵	MeOH	547	665
H ₂ L ¹	1x10 ⁻⁶	DMF	548	646	H ₂ L ²	1x10 ⁻⁶	MeOH	547	665
H ₂ L ¹	1x10 ⁻⁷	DMF	545	642	H ₂ L ²	1x10 ⁻⁷	MeOH	551	666
H ₂ L ¹	1x10 ⁻³	EtOH	551	606	H ₂ L ³	1x10 ⁻³	CH ₃ CN	554	665
H ₂ L ¹	1x10 ⁻⁴	EtOH	548	611	H ₂ L ³	1x10 ⁻⁴	CH ₃ CN	551	656
H ₂ L ¹	1x10 ⁻⁵	EtOH	547	612	H ₂ L ³	1x10 ⁻⁵	CH ₃ CN	550	657
H ₂ L ¹	1x10 ⁻⁶	EtOH	547	613	H ₂ L ³	1x10 ⁻⁶	CH ₃ CN	549	646
H ₂ L ¹	1x10 ⁻⁷	EtOH	551	613	H ₂ L ³	1x10 ⁻⁷	CH ₃ CN	549	659
H ₂ L ¹	1x10 ⁻³	MeOH	554	666	H ₂ L ³	1x10 ⁻³	DMF	547	677
H ₂ L ¹	1x10 ⁻⁴	MeOH	550	667	H ₂ L ³	1x10 ⁻⁴	DMF	548	666
H ₂ L ¹	1x10 ⁻⁵	MeOH	547	665	H ₂ L ³	1x10 ⁻⁵	DMF	546	644
H ₂ L ¹	1x10 ⁻⁶	MeOH	547	666	H ₂ L ³	1x10 ⁻⁶	DMF	546	642
H ₂ L ¹	1x10 ⁻⁷	MeOH	548	666	H ₂ L ³	1x10 ⁻⁷	DMF	547	643
H ₂ L ²	1x10 ⁻³	CH ₃ CN	555	666	H ₂ L ³	1x10 ⁻³	EtOH	545	608
H ₂ L ²	1x10 ⁻⁴	CH ₃ CN	551	662	H ₂ L ³	1x10 ⁻⁴	EtOH	548	611
H ₂ L ²	1x10 ⁻⁵	CH ₃ CN	549	660	H ₂ L ³	1x10 ⁻⁵	EtOH	548	613
H ₂ L ²	1x10 ⁻⁶	CH ₃ CN	547	659	H ₂ L ³	1x10 ⁻⁶	EtOH	547	613
H ₂ L ²	1x10 ⁻⁷	CH ₃ CN	547	659	H ₂ L ³	1x10 ⁻⁷	EtOH	550	613
H ₂ L ²	1x10 ⁻³	DMF	547	674	H ₂ L ³	1x10 ⁻³	MeOH	546	668
H ₂ L ²	1x10 ⁻⁴	DMF	547	665	H ₂ L ³	1x10 ⁻⁴	MeOH	548	666
H ₂ L ²	1x10 ⁻⁵	DMF	548	661	H ₂ L ³	1x10 ⁻⁵	MeOH	547	666
H ₂ L ²	1x10 ⁻⁶	DMF	548	659	H ₂ L ³	1x10 ⁻⁶	MeOH	547	665
H ₂ L ²	1x10 ⁻⁷	DMF	547	651	H ₂ L ³	1x10 ⁻⁷	MeOH	549	665

3.6. Electrochemical Studies

Cyclic voltammetry technique was applied to study the electrochemical properties of H₂L¹-H₂L³ compounds. In these studies, solutions were deposited in volumes of 1x10⁻³ M and 1x10⁻⁴ M in DMF solvent containing 0.1 M Bu₄NBF₄ as electrolyte at 293 K. Measurements were

performed at scan rates in the range of 100–1000 mVs⁻¹, and the obtainable values were determined against an internal ferrocene-ferrocenium standard. All these data are presented in Table 4. The observed cathodic peaks in the cyclic voltammograms correspond to the electrochemical reduction of the azomethine (–CH=N–)

linkage [28]. As supported by the literature, this process typically involves the two-electron/two-proton reduction of the imine group to the corresponding amine moiety ($-\text{CH}_2-\text{NH}-$)[29]. This indicates a semi-reversible or

irreversible behavior, which is significantly influenced by the scan rate and the electronic effects of the substituents on the aromatic ring [30].

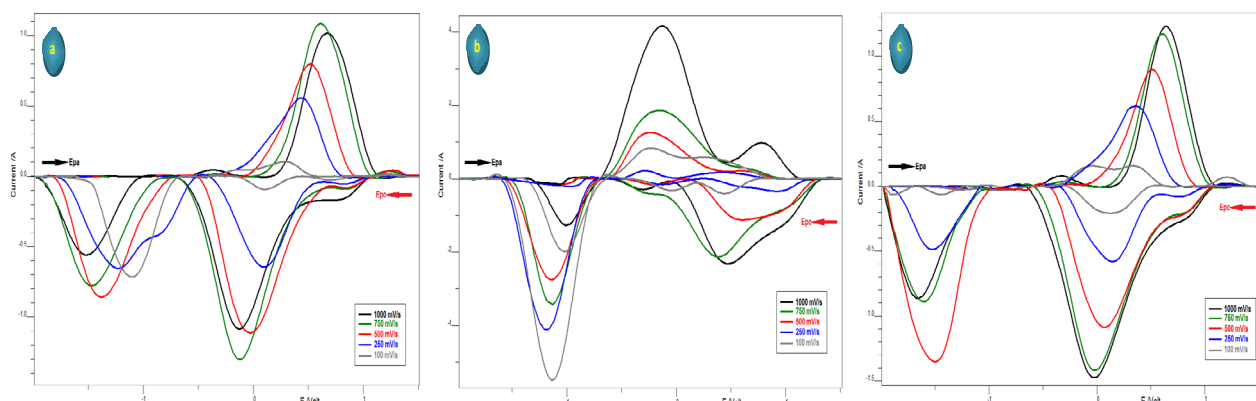


Figure 4. Cyclic voltammograms of H₂L₁ (a), H₂L₂ (b) and H₂L₃ (c) at various scan rates and in 1.0x10⁻³ M DMF solution.

Table 4. Electrochemical data of complex materials.

Compound	Concent.	Solvent	Scan rate (mV s ⁻¹)	E _{pa} (V)	E _{pc} (V)	E _{1/2} (V)	ΔE _p (V)
H ₂ L ¹	1x10 ⁻³	DMF	100	-0.62, -0.14, 0.29	0.71, 0.10, -0.76	-	0.14
			250	0.75, 0.44	0.82, 0.10, -1.23	0.78	0.48
			500	-0.82, -0.30, 0.52	0.84, -0.02, -1.37	-	0.54
			750	-0.79, -0.34, 0.62	0.84, -0.13, -1.48	-	0.69
			1000	-0.36, 0.68	0.76, -0.12, -1.51	0.72	0.80
H ₂ L ¹	1x10 ⁻⁴	DMF	100	-0.69, 0.01, 0.35	0.31, -1.18	0.33	0.04
			250	-0.81, 0.40	0.41, -1.44	0.41	0.63
			500	-0.86, -0.44, 0.56	0.18, -1.57	-	0.38
			750	-0.89, -0.43, 0.61	0.16, -1.59	-	0.45
			1000	-0.90, -0.42, 0.69	0.14, -1.65	-	0.55
H ₂ L ²	1x10 ⁻³	DMF	100	-0.6, -0.03, 0.35, 1.21	0.13, -0.7, -1.45	-	0.10
			250	-0.76, 0.36, 1.25	0.76, 0.16, -0.76, -1.53	0,76	0.20
			500	-0.27, 0.52	0.81, 0.07, -0.87, -1.51	-	0.45
			750	-0.3, 0.61	0.84, -1.01, -1.61	-	0.71
			1000	-0.32, 0.64	0.86, -0.03, -1.06	-	0.74
H ₂ L ²	1x10 ⁻⁴	DMF	100	-0.42, 0.31, 1.16	0.03, -1.09	-	0.28
			250	-0.46, -0.07, 0.49, 1.27	0.87, 0.17	-	0.32
			500	-0.48, 0.57, 1.26	0.91, 0.16	-	0.35
			750	-0.47, 0.62	0.16, -0.47	0.47	0.46
			1000	-0.45, 0.68	0.15, -0.52	-	0.07
H ₂ L ³	1x10 ⁻³	DMF	100	-0.60, 0.28, 1.23	0.71, 0.10, -0.78	-	0.18
			250	-0.40, 0.38, 0.96	0.79, 0.17, -0.32	0.87	0.17
			500	-0.78, -0.06, 0.82	0.60, -0.55	-	0.22
			750	-0.49, 0.63	0.75, 0.19, -0.47	0.48	0.44
			1000	-0.52, 0.67	0.65, -0.52	0.66	0.02
H ₂ L ³	1x10 ⁻⁴	DMF	100	-0.82, -0.02, 0.75, 1.23	0.31, -0.04, -1.25	-	0.44
			250	-0.73, 0.07	0.75, 0.28, -0.64, -1.32	0.68	0.59
			500	-0.49, 0.14, 0.53	0.85, 0.21, -1.42	-	0.32
			750	-0.48, 0.19, 0.58	0.17, -0.46, -1.49	0,18	0.02
			1000	-0.48, 0.23, 0.61	0.17, -0.5, -1.55	-	0.06

Voltammetric measurements were carried out against an Ag⁺/AgCl reference electrode in the range of -2.0 V to 2.0 V. Voltammograms of selected ligands H₂L¹ (a) and H₂L³ (b) are presented in Figure 4. Compounds H₂L¹, H₂L² and H₂L³ exhibit reversible redox process at 100, 250, 750 and 1000 mV/s scan rates in both concentrations. In other words, these ligands have irreversible property at the 500 mV/s scan rate. In the redox processes, the imine groups reduce to the amine derivatives by the electron accepting

[31]. However, the ligand H₂L² shows the only one reversible process at the 750 mV/s scan rate. In other all conditions, the ligand has the irreversible redox properties. As the scan rate is increase, the redox potentials shifted to the positive regions. Because of OH groups on the benzene rings give electron to ring by the mesomeric effect, the redox processes have been occurred at low potentials.

3.7. Surface Analysis

To do the surface analyses of the microspheres, their SEM images were investigated. Figure 5 shows the SEM images of initial Merrifield resin microspheres (PS). When the Figure 5 investigated, the surface of PS microspheres is very smooth. Whereas the SEM images of the polymer-

attached Schiff bases show slight roughening of the top layer because on the surfaces of PS microspheres the surface modification reactions have occurred. The morphology of catalyst microspheres of PS-Lⁿ-M(II) [n: 1, 2, 3; M: Cu (II), Ni (II), Co (II)] is like that of PS-H₂Lⁿ microspheres, and the surface seems slight rough.

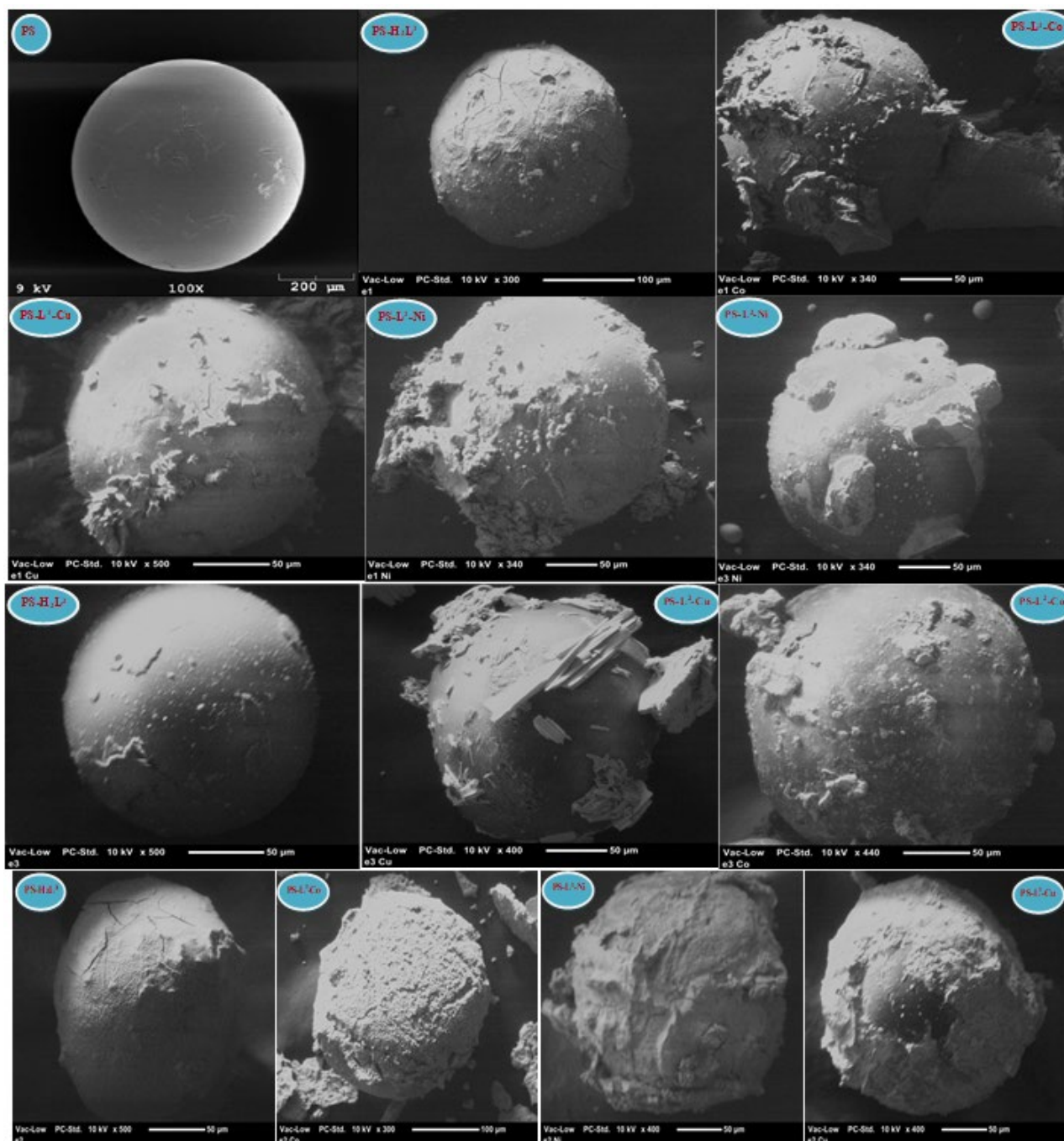


Figure 5. SEM images of Merrifield peptide resin (PS), (PS-H₂L¹), (PS-L¹-Co), (PS-L¹-Cu), (PS-L¹-Ni), (PS-H₂L²), (PS-L²-Co), (PS-L²-Cu), (PS-L²-Ni), (PS-H₂L³), (PS-L³-Co), (PS-L³-Cu) and (PS-L³-Ni) microspheres.

When the smooth PS microsphere bonded with the H₂L¹ ligand, it showed a homogeneous distribution, and no agglomeration or clustering was observed. When the PS-H₂L¹ material formed because of binding with the H₂L¹ ligand forms a complex structure with Co metal, clusters and clusters are observed in the SEM microsphere image of the complex compound. This image shows that the PS-supported Schiff base material successfully forms a complex structure with the metal atom. Similarly, it is observed that the PS-H₂L¹ material

exhibits regular complexation with Cu and Ni metal atoms. When the SEM microspheres of the complex materials formed by the PS-H₂L² material with Co, Cu and Ni atoms are examined, it is observed that they exhibit quite different bonding. While regular complexation is observed with Co metal, it is observed that Cu metal exhibit's regular crystalline structure by forming agglomeration and clustering in various parts of the material. It is observed that it forms clusters with Ni metal in some places. When the SEM microsphere images

of the complex structure formed by the PS-H₂L³ material with Co, Cu and Ni metal atoms are examined, it is observed that the regular agglomerations exhibit a more spread-out distribution rather than clusters that exhibit a more homogeneous distribution. SEM images of microspheres of PS-H₂L², PS-L²-Co, PS-L²-Cu and PS-L²-Ni with (PS-H₂L³), (PS-L³-Co), (PS-L³-Cu) and (PS-L³-Ni) compounds are given in Figure 5.

3.8. Thermal Studies

Thermal properties of the polymer-attached materials and their Co²⁺, Ni²⁺ and Cu²⁺ metal complexes were researched in the 20-1000 °C temperature range nitrogen surroundings at a heating degree of 10 °C/min. Thermal curves of the polymer attached Schiff base ligand PS-H₂L², PS-H₂L³, PS-L¹-Ni(II) and PS-L²-Ni(II) complexes were given in Figure 6.

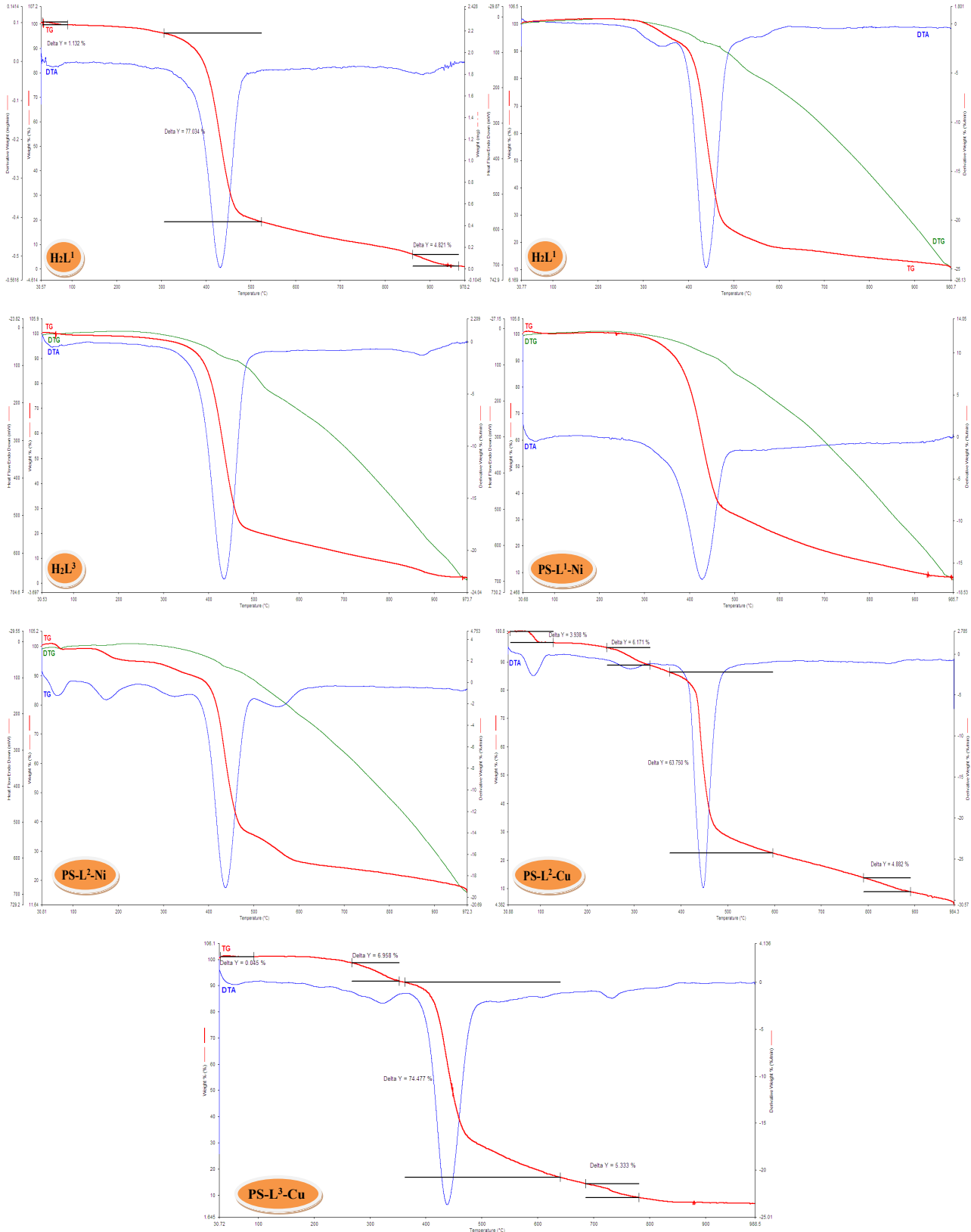


Figure 6. Thermal curves of H₂L¹, H₂L² and H₂L³ Schiff base ligands & (PS-L¹-Ni), (PS-L²-Ni), (PS-L²-Cu) and (PS-L³-Cu) complexes in temperature range of 10–1000 °C.

3.9. Catalytic Studies

Table 5. Catalytic oxidation of C₆H₁₂ (CyH) and C₈H₁₆ with H₂O₂^a in microwave irradiation environment^b.

Compounds.	%Conv	%Cy-OH	%Cy=O	%Conv	%CyON-OH	%CyON=O
PS-L ¹ -Co (II)	0.7	0.6	0.1	81.2	6.5	0.8
PS-L ¹ --Cu (II)	4.9	2.1	2.8	87.5	1.2	2.6
PS-L ¹ --Ni (II)	5.9	5.4	0.5	81.9	0.1	0.5
PS-L ² -Co (II)	49.8	21.2	2.4	81.2	0.7	3.7
PS-L ² -Cu (II)	64.7	13.4	4.5	86.3	0.7	0.2
PS-L ² -Ni (II)	59.0	11.7	1.2	86.0	1.0	1.5
PS-L ³ -Co (II)	49.9	2.3	0.3	91.7	0.1	0.2
PS-L ³ -Cu (II)	61.9	0.6	2.3	87.4	0.5	1.8
PS-L ³ -Ni (II)	35.0	1.1	0.2	81.2	0.2	0.8

a: (0.02 mmol catalyst)/2 mmol substrate (C₆H₁₂ or C₈H₁₆)/3 mmol H₂O₂ (1/100/150) and 5 mL acetonitrile was used for each reaction. b: During the reaction, it is maintained at a temperature of around 140 °C and a pressure of 30 bar in closed DAP60 vessels, with a power resistance of 400 W for 60 minutes.

Determination of the optimum rate of reactions of C₆H₁₂, C₈H₁₆, C₆H₁₀ and styrene are based on the effects of temperature, pressure, excipients, reaction time and dissolution rates.

Investigations of oxidation rates at 140°C indicated that large amounts did not significantly affect the overall conversion of C₆H₁₂ and C₈H₁₆ but enhanced their conversion to cyclic alcohols and ketones. The loss of metal atoms and cleavage during the reaction and storage processes contributes to the observed activity cessation.

The polymer-attached Schiff base ligands used in this complex enhance the *p*-electron properties of the ring through the mesomeric effect, thanks to -OH group in the para position of salicylidene moiety. Optimized reaction conditions obtained from these studies successfully completed the oxidation reactions of C₆H₁₂ and C₈H₁₆ in the combined units of solid-supported Schiff base metal complexes, and these details are presented in Table 5. The oxidation curves of the PS-L²-M(II) and PS-L³-M(II) solid support metal complexes were given in Figure 7.

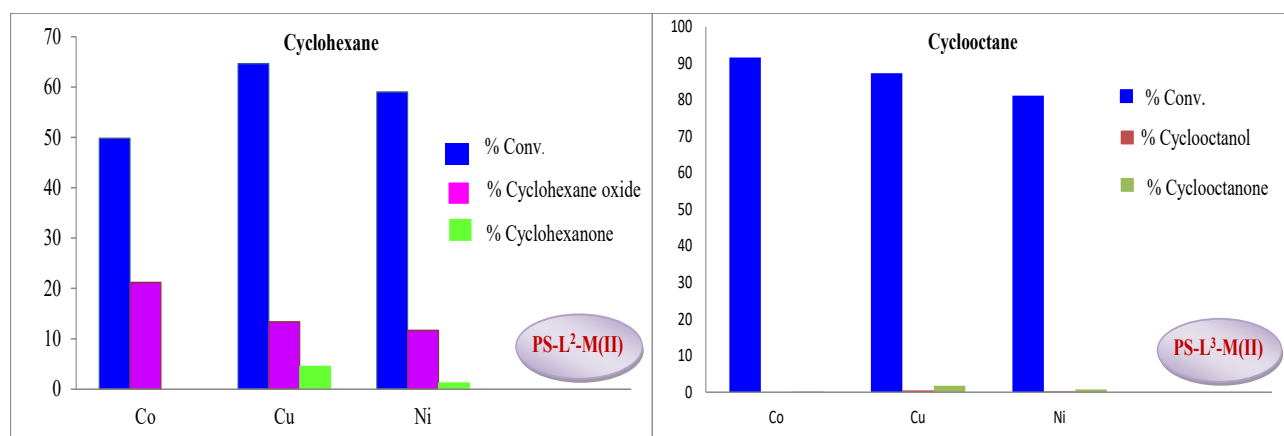


Figure 7. PS-L²-M(II) and PS-L³-M(II) for alkane-oxidation. Effect of complexes on the oxidation of C₆H₁₂ and C₈H₁₆ in microwave radiation environment. 0.02 mmol catalyst: 2 mmol C₆H₁₂/ C₈H₁₆: 4 mmol H₂O₂ 1/100/200 and 5 mL acetonitrile were used for each reaction. Throughout the reaction, the temperature was maintained at approximately 100°C and the pressure at 30 bar in closed DAP60 vessels, while 300 W power was applied for 30 minutes.

The direct functionalization of inactive C-H bonds in saturated hydrocarbons under harsh reaction conditions, often high pressure and temperature, is of particular interest in this field. In this study, the highest yields were obtained at 400 W microwave power for 60 min. These optimum conditions included acetonitrile solvents and mole ratios of 1/100/200 (catalyst:substrate:oxidant). The reaction temperature was approximately 140 °C and the pressure was 30 bar. As a control group, an uncoupled

blank experiment was performed with the same processes. According to the possible conversion rates, the first and slowest step is the addition of CyH and CyON to cyclic alcohols and ketones. Controlling this first step is crucial for improving the selection of targeted products, such as (Cy-OH), (Cy=O), (CyON-OH), and 8CyON=O. The final reaction products obtained under microwave irradiation with H₂O₂ and a customized reaction method are shown in detail in Figure 8.

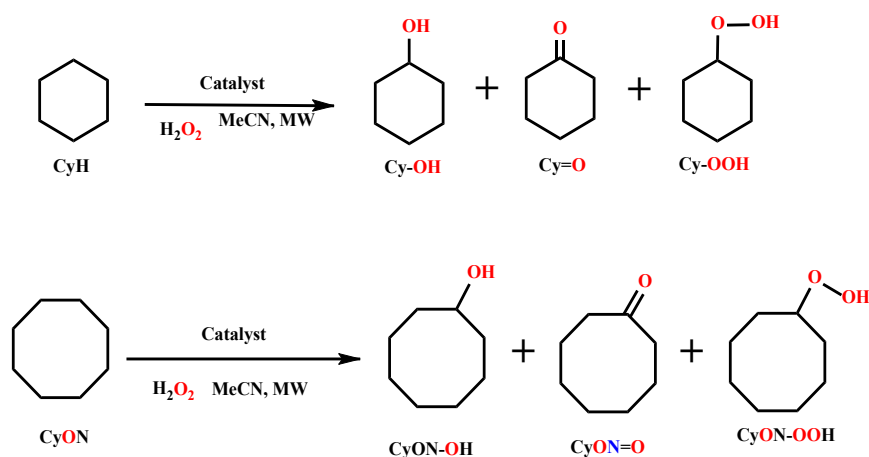


Figure 8. Formed products in alkane-oxidation reactions.

Oxidation reactions occur around the metal centers of the complexes. Microwave power and newer power sources have been suggested to have the potential to selectively convert CyH to (Cy-OH) and (Cy=O), and (CyON) to (CyON-OH) and (CyON=O). The synthesized polymer supported Schiff base complex PS-L²-Cu (II) showed the highest activity for the CyH to (Cy-OH) and (Cy=O). In the other hand, the PS-L¹-Co (II) complex has the lowest activity for the C₆H₁₂ oxidation. In the C₈H₁₆ oxidation reactions, while the PS-L³-Co (II) has the highest activity and PS-L³-Ni (II) complex has also lowest catalytic activity. The important point in conversion of the C₆H₁₂ or C₈H₁₆ to the oxidized products is the reduction of M(II)-L to M(I)-L (L: ligand). The tetrahedral geometry of the Cu (II) complex

is considered a possible reason for its higher activity compared to other complexes. This structure facilitates the disintegration of the M(II)-L complex by ligands of metal cation. Resulting oxidation products, such as (Cy-OH), (Cy=O), (CyON-OH), and (CyON=O), clearly indicate that the explosions carried out a nuclear attack on active bonds.

In the epoxidation reaction, we used styrene and C₆H₁₀ as a substrate. The epoxidation products of the C₆H₁₀ are the cyclohexanol, cyclohexanone and C₆H₁₂ oxide. In the reaction of the styrene, the styrene oxide is the reaction product. The obtained data from the epoxidation reactions are given in Table 6 and the reaction products were shown in Figure 9.

Table 6. Catalytic oxidation of C₆H₁₂ CyH and C₈H₁₆ with H₂O₂ ^a in microwave radiation environment^b

Compounds.	%Conv.	%Cy-OH	%Cy=O	%Cy-ox	%Conv.	%Str-Ox
PS-L ¹ -Co (II)	40.1	19.3	4.2	0.8	37.0	9.3
PS-L ¹ -Cu (II)	69.4	19.2	2.0	0.7	34.1	1.0
PS-L ¹ -Ni (II)	32.2	18.8	2.1	0.4	48.5	0.7
PS-L ² -Co (II)	46.5	21.3	3.6	-	44.5	0.1
PS-L ² -Cu (II)	66.7	20.8	1.2	-	32.3	0.2
PS-L ² -Ni (II)	69.6	20.2	5.9	1.3	49.6	1.4
PS-L ³ -Co (II)	50.5	20.2	7.6	2.2	42.7	1.2
PS-L ³ -Cu (II)	67.5	19.7	2.3	0.5	28.9	0.7
PS-L ³ -Ni (II)	60.6	18.5	1.2	0.1	48.3	2.0

a: (0.02 mmol catalyst)/2 mmol substrate (C₆H₁₀ or C₈H₈):3 mmol H₂O₂ (1:100:150) and 5 mL acetonitrile were used for each reaction. b: A power of 400 W was applied for 60 min. The reaction temperature and pressure were kept constant at approximately 140 °C and 30 bar in closed DAP60 vessels.

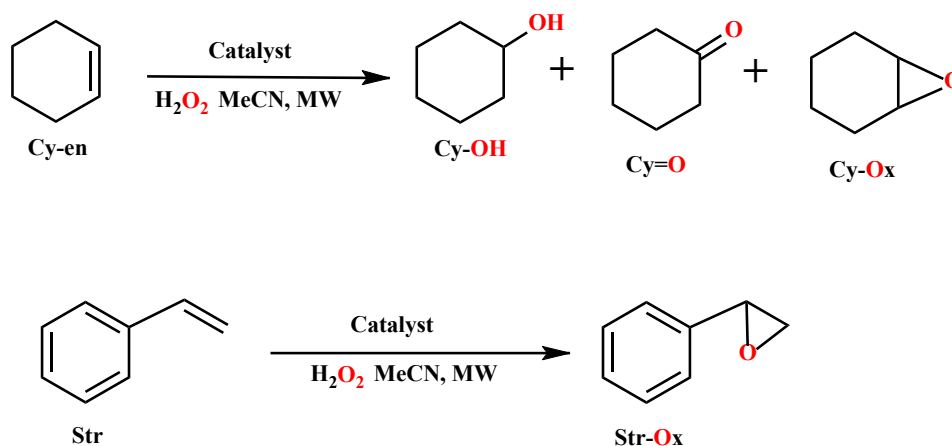


Figure 9. Alkene-epoxidation reactions by the metal catalyst.

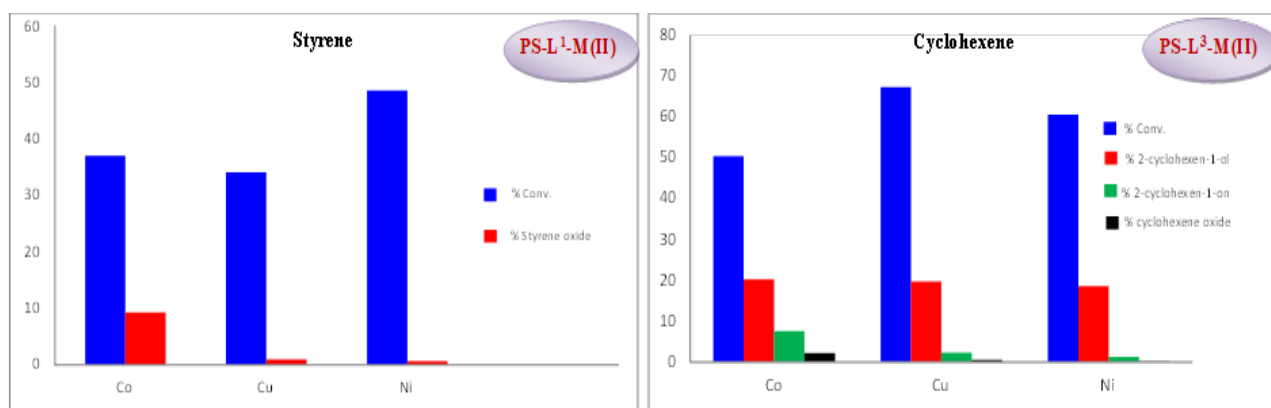


Figure 10. PS-L¹-M(II) and PS-L³-M(II) for epoxidation reaction. The effects of complexes on the oxidation of C₆H₁₀ and styrene under microwave irradiation were investigated. 2 mmol C₆H₁₂ (C₈H₁₆): 0.02 mmol catalyst: 4 mmol H₂O₂ (1/100/200) and 5 mL acetonitrile were used for each reaction. A power of 300W was applied to this reaction, which was carried out in closed DAP60 vessels at approximately 100 °C and 30 bar pressure for 30 minutes.

The oxidation curves of the PS-L¹-M(II) and PS-L³-M(II) solid support metal complexes were given in Figure 10. As seen also from Table 6, in the styrene epoxidation, the PS-L²-Cu (II), PS-L³-Cu (II) and PS-L²-Ni (II) complexes show lowest epoxidation activity. Solid support PS-L¹-Co (II) complex has the highest activity in the styrene epoxidation. In the C₆H₁₀ epoxidation reaction, the PS-L²-Ni (II) polymer complex has the high activity. On the other hand, the PS-L²-Co (II) and PS-L²-Cu (II) polymer complexes have not any activity.

4. Conclusions

This research, we synthesized three polymer-attached Schiff bases PS-H₂L¹-PS-H₂L³ and their Cu (II), Co (II) and Ni (II) transition metal complexes. All materials were described by the spectroscopic and analytical techniques. Electrochemical and photoluminescence values of the ligands H₂L¹-H₂L³ were investigated and some of them have the reversible redox properties. On the photophysical properties of the ligands effect of the different solvents and concentrations. In the alkane-oxidation of polymer-attached metal complexes, the other products from the desired alcohol and ketones were formed. Thermal stability of the polymer-attached and their metal complexes are higher than free ligands H₂L¹-H₂L³. SEM images of polymer-attached Schiff bases show slight roughening of the top layer because on the surfaces of PS microspheres the surface modification reactions have occurred.

In this study, significantly contributes to the field of coordination chemistry and catalysis by expanding the application of polymer-based heterogeneous catalysts. The development of these new types of materials and the detailed study of their catalytic performance contribute to a more detailed understanding of heterogeneous catalysis. Furthermore, their demonstrated effectiveness in industrially important oxidation and epoxidation processes highlights the potential of these thermally stable catalysts for practical chemical synthesis and significantly contributes to the development of new and efficient catalytic systems.

Acknowledgments

We are grateful to the Automatization of KSU Scientific Research Projects (Project No: 2013/1-12 YLS) for the support of this research.

Conflict of Interest

The authors declare that they have no known competing financial interests or personal relationships that could have influenced the work presented in this article.

References

- [1] Aleku, G. A. (2024). Imine Reductases and Reductive Aminases in Organic Synthesis. *ACS Catalysis*, 14(19), 14308–14329. <https://doi.org/10.3390/ijms25042263>
- [2] Yan, Q., Wu, X., Jiang, H., Wang, H., Xu, F., Li, H., Zhang, H., & Yang, S. (2024). Transition metals-catalyzed amination of biomass feedstocks for sustainable construction of N-heterocycles. *Coordination Chemistry Reviews*, 502, 215622. <https://doi.org/10.1016/j.ccr.2023.215622>
- [3] Aziz, K. N., Ahmed, K. M., Omer, R. A., Qader, A. F., & Abdulkareem, E. I. (2024). A review of coordination compounds: structure, stability, and biological significance. *Reviews in Inorganic Chemistry*. <https://doi.org/10.1515/revic-2024-0035>
- [4] Dhanya, T. M., Rajimon, K. J., Mohanan, N. K., Anilkumar, A., Pillai, S. S., & Mohanan, P. V. (2024). Exploring the Enzyme Inhibition Potential of Schiff Base and Metal Complexes of Benzothiophene Derivatives. *Discover Chemistry*, 1(1), 48. <https://doi.org/10.1007/s44371-024-00048-0>
- [5] Nidhi, Siddharam, Rao, D. P., Gautam, A. K., Verma, A., & Gautam, Y. (2025). Schiff bases and their possible therapeutic applications: A review. *Results in Chemistry*, 13, 101941. <https://doi.org/10.1016/j.rechem.2024.101941>
- [6] de França, I. V., Döring, T. H., de Oliveira Neto, F. M., Pedroso, M. J., & da Cruz Júnior, J. W. (2024). Imines and their metal complexes as active drugs against Chagas disease: A review in recent years and analyses of in silico properties. *Journal of Molecular Structure*, 1314, 138725. <https://doi.org/10.1016/j.molstruc.2024.138725>
- [7] Kainat, S. F., Hawsawi, M. B., Mughal, E. U., Naeem, N., Almohyawi, A. M., Altass, H. M., Hussein, E. M., Sadiq, A., Moussa, Z., Abd-El-Aziz, A. S., & Ahmed, S. A. (2024). Recent developments in the synthesis and applications of terpyridine-based metal complexes: a systematic review. *RSC Advances*, 14(30), 21464–21537. <https://doi.org/10.1039/D4RA04119D>
- [8] Anane, J., Owusu, E., Rivera, G., & Bandyopadhyay, D.

- (2024). Iron–Imine Cocktail in Drug Development: A Contemporary Update. *International Journal of Molecular Sciences*, 25(4), 2263. <https://doi.org/10.3390/ijms25042263>
- [9] Bhat, M. A., Bhat, S. A., Alabada, R., Kaur, M., Kaur, H., Prasad, G. V. S., Verma, R., Dev, A., Gupta, M., Sinha, A., Dahlous, K. A., & Butcher, R. J. (2024). Effect of hydroxy groups on structural, electronic, and biological properties of methyl carbazate containing hydroxy benzaldehyde-based imines. *Journal of Molecular Structure*, 1311, 138376. <https://doi.org/10.1016/j.molstruc.2024.138376>
- [10] Goshisht, M. K., Patra, G. K., & Tripathi, N. (2022). Fluorescent Schiff base sensors as a versatile tool for metal ion detection: strategies, mechanistic insights, and applications. *Materials Advances*, 3(6), 2612–2669. <https://doi.org/10.1039/D1MA01175H>
- [11] Farokhi, A., Lipinski, S., Cavinato, L. M., Shahroosvand, H., Pashaei, B., Karimi, S., Bellani, S., Bonaccorso, F., & Costa, R. D. (2025). Metal complex-based TADF: design, characterization, and lighting devices. *Chemical Society Reviews*, 54(1), 266–340. <https://doi.org/10.1039/D3CS01102J>
- [12] Tawfiq, K. M., Al Naymi, H. A. S., Obaid, S. M. H., Jarad, A. J., Al-Noor, T. H., & Al-Sarray, A. J. (2025). Synthesis, Characterization, Molecular Docking, Cytotoxicity, and Antimicrobial Activity of Schiff Base Ligand and Its Metal Complexes. *Applied Organometallic Chemistry*, 39(1). <https://doi.org/10.1002/aoc.7781>
- [13] Khabibjonovich, A. A., Yusupboevich, Y. Y., Zamirovich, A. B., Khamidjanovich, R. A., Sadullayevich, N. A., Behzodjon, M. D., Kodamboevich, K. P., Abdullaev, I. I., Balakrishnan, C., Tulaganovich, I. B., Mengnorovich, A. J., Gao, J., & Bakhtiyarovich, I. A. (2025). Two dimensional coordination polymer of pb(II) complex with m-sulfanilic acid. *Adsorption*, 31(2), 32. <https://doi.org/10.1007/s10450-024-00587-z>
- [14] Wu, S., Huang, X., Fu, S., Li, Z., Yin, S., Liao, W., Wang, M., Lu, Y., Bonn, M., Sun, Y., Feng, X., & Xu, W. (2025). Selenium-Substitution Strategy for Enhanced Mobility, Tunable Bandgap, and Improved Electrochemical Energy Storage in Semiconducting Conjugated Coordination Polymers. *Angewandte Chemie International Edition*. <https://doi.org/10.1002/anie.202419865>
- [15] Peng, L., Odnoroh, M., Destarac, M., Coppel, Y., Delmas, C., Benoit-Marquié, F., Mingotaud, C., & Marty, J.-D. (2025). How tailor-made copolymers can control the structure and properties of hybrid nanomaterials: the case of polyionic complexes. *Nanoscale*. <https://doi.org/10.1039/D4NR04332D>
- [16] Zhao, Z., Melinte, G., Lei, Y., Guo, D., Hedhili, M. N., Shi, Z., Qasem, H., & Alshareef, H. N. (2025). New Dissolution Chemistry of Nylon Promises Reversible Li-Metal Batteries. *ACS Energy Letters*, 1129–1138. <https://doi.org/10.1021/acsenergylett.4c03221>
- [17] Blasco, E., Sims, M. B., Goldmann, A. S., Sumerlin, B. S., & Barner-Kowollik, C. (2017). 50th Anniversary Perspective: Polymer Functionalization. *Macromolecules*, 50(14), 5215–5252. <https://doi.org/10.1021/acs.macromol.7b00465>
- [18] Qin, C., Wang, Y., Hu, J., Wang, T., Liu, D., Dong, J., & Lu, Y. (2023). Artificial Olfactory Biohybrid System: An Evolving Sense of Smell. *Advanced Science*, 10(5). <https://doi.org/10.1002/adv.202204726>
- [19] Zhang, Z., Lu, Y., Zhao, Y., Cui, L., Xu, C., & Wu, S. (2025). Current Developments in Chitosan-Based Hydrogels for Water and Wastewater Treatment: A Comprehensive Review. *ChemistrySelect*, 10(6). <https://doi.org/10.1002/slct.202404061>
- [20] Wang, S., Li, J., Ren, F., Zhang, J., Song, W., & Ren, L. (2025). New Dawn in the Treatment of Rheumatoid Arthritis: Advanced Insight into Polymer Hydrogel Research. *Gels*, 11(2), 136. <https://doi.org/10.3390/gels11020136>
- [21] Moulay, S. (2018). Functionalized Polystyrene and Polystyrene-Containing Material Platforms for Various Applications. *Polymer-Plastics Technology and Engineering*, 57(11), 1045–1092. <https://doi.org/10.1080/03602559.2017.1370109>
- [22] Kaliyappan, T., & Kannan, P. (2000). Co-ordination polymers. *Progress in Polymer Science*, 25(3), 343–370. [https://doi.org/10.1016/S0079-6700\(00\)00005-8](https://doi.org/10.1016/S0079-6700(00)00005-8)
- [23] Dolaz, M., McKee, V., Gölcü, A., & Tümer, M. (2009). Synthesis, structural characterization, thermal and electrochemical studies of the N,N'-bis[(3,4-dichlorophenyl)methylidene]cyclohexane-1,4-diamine metal complexes. *Spectrochimica Acta Part A: Molecular and Biomolecular Spectroscopy*, 71(5), 1648–1654. <https://doi.org/10.1016/j.saa.2008.06.012>
- [24] Daştan, A., Kulkarni, A., & Török, B. (2012). Environmentally benign synthesis of heterocyclic compounds by combined microwave-assisted heterogeneous catalytic approaches. *Green Chemistry*, 14(1), 17–37. <https://doi.org/10.1039/C1GC15837F>
- [25] Wang, D., & Astruc, D. (2017). The recent development of efficient Earth-abundant transition-metal nanocatalysts. *Chemical Society Reviews*, 46(3), 816–854. <https://doi.org/10.1039/C6CS00629A>
- [26] Gennari, C., & Piarulli, U. (2003). Combinatorial Libraries of Chiral Ligands for Enantioselective Catalysis. *Chemical Reviews*, 103(8), 3071–3100. <https://doi.org/10.1021/cr020058r>
- [27] Maurya, A. (2026). Carbonaceous supports for Schiff base metal complexes: Strategies for enhanced catalytic efficiency. *iScience*, 29(3), 114688. <https://doi.org/10.1016/j.isci.2026.114688>
- [28] Kamaci, M., & Kaya, İ. (2014). Synthesis, Thermal and Morphological Properties of Polyurethanes Containing Azomethine Linkage. *Journal of Inorganic and Organometallic Polymers and Materials*, 24(5), 803–818. <https://doi.org/10.1007/s10904-014-0046-8>
- [29] Kumar Jha, R., & Kumar, S. (2024). Direct Functionalization of para-Quinones: A Historical Review and New Perspectives. *European Journal of Organic Chemistry*, 27(27). <https://doi.org/10.1002/ejoc.202400535>
- [30] Orselli, E., Kottas, G. S., Konradsson, A. E., Coppo, P., Fröhlich, R., De Cola, L., van Dijken, A., Büchel, M., & Börner, H. (2007). Blue-Emitting Iridium Complexes with Substituted 1,2,4-Triazole Ligands: Synthesis, Photophysics, and Devices. *Inorganic Chemistry*, 46(26), 11082–11093. <https://doi.org/10.1021/ic701110p>
- [31] Ceyhan, G., Köse, M., McKee, V., Uruş, S., Gölcü, A., & Tümer, M. (2012). Tetradentate Schiff base ligands and their complexes: Synthesis, structural characterization, thermal, electrochemical and alkane oxidation. *Spectrochimica Acta Part A: Molecular and Biomolecular Spectroscopy*, 95, 382–398.